

# Reconstruction and classification of tau lepton decays with ILD

T.H. Tran <sup>a,1</sup>, V. Balagura <sup>1</sup>, V. Boudry <sup>1</sup>, J.-C. Brient<sup>1</sup>, H. Videau <sup>1</sup>

<sup>1</sup>Laboratoire Leprince-Ringuet, École polytechnique, CNRS/IN2P3, Université Paris-Saclay, 91128 Palaiseau, France

the date of receipt and acceptance should be inserted later

**Abstract** Tau-lepton decays with up to two  $\pi^0$ 's in the final state,  $\tau^+ \rightarrow \pi^+ \bar{\nu}_\tau$ ,  $\rho^+ (\pi^+ \pi^0) \bar{\nu}_\tau$ ,  $a_1^+ (\pi^+ \pi^0 \pi^0) \bar{\nu}_\tau$ , are used to study the performance of the barrel part of the silicon-tungsten electromagnetic calorimeter (Si-W ECAL) of International Large Detector (ILD) at the future  $e^+ - e^-$  International Linear Collider. A correct reconstruction of the tau decay mode is crucial for constraining the tau spin state and measuring the Higgs boson CP state in  $H \rightarrow \tau^+ \tau^-$  decays. About 95% of  $\pi^+ \bar{\nu}_\tau$  and 90% of  $\rho^+ \bar{\nu}_\tau$  and  $a_1^+ \bar{\nu}_\tau$  decays from  $e^+ e^- \rightarrow Z^0 \rightarrow \tau^+ \tau^-$  reaction at  $e^\pm$ -beam energy of 125 GeV are correctly reconstructed. In a smaller ILD detector, with Si-W ECAL radius reduced by about 20% these numbers degrade by at most 2%. The  $\pi^0$  mass resolution stays below 10%. Since the failures in the tau-lepton reconstruction are mainly due to photons, the increase of the ILD magnetic field from 3.5 T to 4 T does not bring any significant improvement.

## 1 Introduction

The tau-lepton decays have been used at LEP [1] and many other experiments for precise tests of the Standard Model. The tau spin state can be inferred from its decay mode and the momenta of all reconstructed decay products [2]. This will be used at the future lepton colliders, for example, to measure the CP (the product of charge conjugation and parity symmetries) state of the Higgs boson decaying into a tau pair,  $H^0 \rightarrow \tau^+ \tau^-$ . In average, the tau decay products are more collimated than the QCD jets of similar energy, and the separation of photon clusters in the electromagnetic calorime-

ter (ECAL) is more difficult. Incorrect determination of the number of photons in the tau final state results in the wrong reconstruction of the tau decay mode and spoils the spin state measurement. This provides a thorough test of the ECAL performance.

In this paper we study the reconstruction and classification of  $\tau^+$  decay modes in the International Large Detector (ILD), a proposed detector concept for the  $e^+ - e^-$  International Linear Collider (ILC). We concentrate on the reconstruction of three main tau decays with one charged pion<sup>1</sup> and up to two  $\pi^0$ 's:  $\tau^+ \rightarrow \pi^+ \bar{\nu}_\tau$ ,  $\rho^+ \bar{\nu}_\tau$ ,  $a_1^+ \bar{\nu}_\tau$  followed by  $\rho^+ \rightarrow \pi^+ \pi^0$ ,  $a_1^+ \rightarrow \pi^+ \pi^0 \pi^0$  and  $\pi^0 \rightarrow \gamma\gamma$ . For simplicity, we study almost monochromatic tau-leptons from the decay of the virtual  $Z^0$ ,  $e^+ e^- \rightarrow Z^0 \rightarrow \tau^+ \tau^-$  at  $e^\pm$ -beam energy of 125 GeV. This corresponds to 250 GeV centre-of-mass energy up to beamstrahlung and radiative corrections. The tau-lepton momenta in this reaction are larger than, for example, in  $e^+ e^- \rightarrow H^0 Z^0$ ,  $H^0 \rightarrow \tau^+ \tau^-$  at the same centre-of-mass energy. Therefore, our results correspond to the Higgs boson production at higher ILC energies.

Only the task of the correct classification of three  $\tau^+$  decay modes above is considered in this paper. Neither backgrounds are simulated (they are expected to be small at ILC), nor any attempt is made to calculate  $\tau^+$  spin state from the momenta of the reconstructed decay products.

The ILD detector is optimized for the particle flow algorithm approach (PFA) [3, 4]. It combines the tracker systems with little amount of material and highly granular, “imaging” calorimeters. A complete description of ILD is given in [5, 6]. In this study the ILD performance with a baseline design is simulated with the

<sup>a</sup>e-mail: trong.hieu.tran@llr.in2p3.fr

<sup>1</sup>The inclusion of charge-conjugate states is implied in this article.

software framework MOKKA [7] with a parametric geometry description, based on the GEANT4 package [8]. The charged pion from  $\tau^+$  decay is reconstructed in ILD silicon vertex and tracker detectors and the time projection chamber. The photon clusters are reconstructed in the ILD silicon-tungsten sampling electromagnetic calorimeter (Si-W ECAL). We limit our analysis to the barrel part of ECAL, to avoid complications in the region of barrel – endcap overlap. The hadronic calorimeter is not used.

Si-W ECAL has about 23 radiation lengths. The silicon sensors have a pixelization of  $5 \times 5 \text{ mm}^2$  and a thickness of  $500 \text{ }\mu\text{m}$ . Due to their high cost and large area, Si-W ECAL is one of the most expensive subdetectors in ILD. Several studies of its cost optimization have been performed. In [6] it has been shown that a reduction of the number of ECAL layers from 30 to 26 degrades the jet energy resolution by less than 5% in a jet energy range of 45–250 GeV. In a more recent paper [9], it was demonstrated that a reduction of the ECAL radius by about 20% degrades the jet energy resolution by at most 8% in the same energy range, while the total price of ILD could be lowered by a factor of 1.5.

The current paper supplements the latter optimization study. In addition to the baseline ILD design with the ECAL inner radius of 1843 mm, we present results on the tau decay mode reconstruction in smaller ILD with the ECAL radii of 1615 and 1450 mm. These numbers have been chosen according to the size of the large industrially available silicon sensors in order to simplify the final ECAL mechanical design. The ECAL length is also reduced in order to preserve the same radius-over-length aspect ratio. All other detector parameters, like ECAL total and layer thicknesses, pixel size, gap between the barrel and the endcaps, etc., are unchanged.

The degradation of the jet and the track momentum resolution in smaller ILD may be compensated by a higher magnetic field. Therefore, we also simulated the ILD performance with the magnetic field increased from the nominal 3.5 to 4 T.

## 2 Simulation and Reconstruction

We used a sample of  $e^+e^- \rightarrow Z^0 \rightarrow \tau^+\tau^-(\gamma)$  decays at 250 GeV produced for the ILD “Detailed Baseline Design” report included in the ILC “Technical Design Report” [6]. The tau decay is generated by the TAUOLA library [10]. Events with an initial state radiation are removed at a generator level, but the final state radiation (FSR),  $Z^0 \rightarrow \tau^+\tau^-\gamma$ , is retained. FSR in the tau decays,  $\tau^+ \rightarrow \pi^+\bar{\nu}_\tau\gamma$ ,  $\rho^+\bar{\nu}_\tau\gamma$ ,  $a_1^+\bar{\nu}_\tau\gamma$ , is also retained. The tau branching fractions of the three decays under study without FSR are listed in Table 1. They

Decay mode	Branching fraction [%]
$\pi^+\bar{\nu}_\tau$	$10.83 \pm 0.06$
$\rho^+\bar{\nu}_\tau$ ( $\rho^+ \rightarrow \pi^+\pi^0$ )	$25.52 \pm 0.09$
$a_1^+\bar{\nu}_\tau$ ( $a_1^+ \rightarrow \pi^+\pi^0\pi^0$ )	$9.30 \pm 0.11$

Table 1: Branching fractions of three tau decays under study with one charged and up to two neutral pions in the final state [11].

cover 45% of all tau decay modes and about 70% of the hadronic decays.

Each of the two  $\tau$ -leptons is reconstructed only inside the hemisphere defined by an axis pointing in the tau direction in the  $Z^0$  rest frame. The events with a photon conversion before ECAL are filtered out by requiring that only one charged track is reconstructed in each hemisphere.

### 2.1 The GARLIC clustering algorithm

The Gamma Reconstruction at a Linear Collider Experiment (GARLIC) package [12, 13], version 3.0.3, is used to find photon clusters. The calibration constants for converting the energy deposited in the silicon sensors to the full photon energy are determined using samples of 10 GeV photons. This is done separately for the baseline and two smaller ILD ECAL models to take into account the possible variation of the overall weight of non-instrumented ECAL zones. The difference between the calibration constants for all three models is less than 1%.

### 2.2 Photon identification

The final identification of photon clusters is performed using not GARLIC package but a specialized algorithm described below. It is developed for the purposes of this analysis.

FSR photons are suppressed by requiring the photon energy to be greater than 0.5 GeV. This eliminates 70% of FSR photons and only 6% of photons from  $\tau^+ \rightarrow \rho^+\bar{\nu}_\tau$ ,  $a_1^+\bar{\nu}_\tau$  decays.

To distinguish the genuine photons from fake clusters, for example, originating from the charged  $\pi^+$  hadronic showers, a boosted decision tree (BDT) is used with the following input variables:

- the distance from the cluster barycentre to the  $\pi^+$  track at the ECAL front surface,
- the cluster depth computed from the cluster start found by the GARLIC algorithm,

- the cluster transverse fractal dimension defined as the logarithm of the number of hits in the cluster,  $N_1$ , divided by the number of hits when the pixels are grouped into larger pseudo-cells of  $4 \times 4$  pixels,  $N_4$ :

$$FD_4 = \log(N_1/N_4)/\log(4). \quad (1)$$

The fractal dimension, introduced in [14], reflects the shower density which is higher in electromagnetic showers.

- The hit energy distribution mean and the standard deviation,
- the fraction of energy deposited between 5 and 10 radiation lengths after the cluster start.

25% of all tau decays are used to train BDT, which is then applied to the remaining 75% of statistics. The photon clusters where more than 50% of hit energy is produced by the true Monte Carlo photon from the tau decay, are used as a signal for a BDT training. The rest of the clusters in the same data sample serves as background.

The number of photons from  $\tau^+$  decay without FSR should be even. Sometimes, three photons are reconstructed, however. This can happen if one of the photon clusters from  $\tau^+ \rightarrow \rho^+ \bar{\nu}_\tau$ ,  $\rho^+ \rightarrow \pi^+ \pi^0$ ,  $\pi^0 \rightarrow \gamma\gamma$  decays is split into two, or this decay is accompanied by the FSR photon. The other possibility is the merging of two photon clusters out of four from  $\tau^+ \rightarrow a_1^+ \bar{\nu}_\tau$ ,  $a_1^+ \rightarrow \pi^+ \pi^0 \pi^0$  decay or loss of one photon. In the first case of  $\tau^+ \rightarrow \rho^+ \bar{\nu}_\tau$  decay, the photon with the minimal energy is soft and the asymmetry between maximal and minimal energies of three photons, defined as

$$A = \frac{E_\gamma^{\max} - E_\gamma^{\min}}{E_\gamma^{\max} + E_\gamma^{\min}}, \quad (2)$$

peaks at one. The distribution of  $A$  for both  $\tau^+ \rightarrow \rho^+ \bar{\nu}_\tau$  and  $a_1^+ \bar{\nu}_\tau$  is shown in Fig. 1a. In this special case of three photons, if  $A > 0.8$ , the energy of the least energetic photon cluster is added to the most energetic one and the cluster is removed from the following analysis.

As a cross-check, the same asymmetry  $A$  is plotted in Fig. 1b in the case of two reconstructed photons. It is dominated by  $\tau^+ \rightarrow \rho^+ \bar{\nu}_\tau$  decays. Since  $\pi^0$  has no spin, its decay products should have a flat asymmetry distribution, ranging from zero to one as the photon is massless. This is really the case for the true Monte Carlo photon energies up to acceptance and detector cut-off effects at one (the solid curve in Fig. 1b). The dashed curve, obtained after reconstruction, shows, however, that the clustering algorithm tends to favor an asymmetric energy partition between the two close photons.

### 2.3 Classification of tau decay modes

To distinguish three  $\tau^+$  decay modes, the second BDT, with gradient boost is used with the following input variables:

- the invariant mass of all reconstructed  $\tau^+$  decay products,  $M_{\text{reco}}$ ,
- the number of reconstructed photons and
- their total invariant mass,
- the energy of the photons and
- their distance from the reconstructed track at the ECAL front surface.

For every decay mode a BDT is trained on 25% of statistics using this decay as a signal and the other two as a background. Three classifiers, obtained in this way (one for every mode), are applied to the remaining 75% of events.

If  $M_{\text{reco}}$  is larger than the tau-lepton mass, the event is rejected, except if it is classified as  $\pi^+ \bar{\nu}_\tau$  with one reconstructed photon. In the latter case it is assumed that the mass beyond the kinematical limit is due to an external FSR photon and the event is accepted.

A small fraction of events is accepted at the same time by two classifiers, mainly when the final state with three reconstructed photons is compatible with both  $\rho^+ \bar{\nu}_\tau$  and  $a_1^+ \bar{\nu}_\tau$  decays. Then, the final decision is made based on  $M_{\text{reco}}$ :  $\rho^+ \bar{\nu}_\tau$  is preferred over  $a_1^+ \bar{\nu}_\tau$  if  $M_{\text{reco}} < 0.85$  GeV and vice versa. For events accepted at the same time by two other classifiers ( $\pi^+ \bar{\nu}_\tau$  and  $\rho^+ \bar{\nu}_\tau$  or  $\pi^+ \bar{\nu}_\tau$  and  $a_1^+ \bar{\nu}_\tau$ ), the preference is made in favor of the heavier particle in the final state. No event passes all three classifiers.

### 3 Results and conclusions

Fig 2 summarizes the probability of the correct reconstruction of tau decay modes  $\tau^+ \rightarrow \pi^+ \bar{\nu}_\tau$ ,  $\rho^+ \bar{\nu}_\tau$  and  $a_1^+ \bar{\nu}_\tau$  in the absence of backgrounds in the barrel Si-W ECAL region. The results are presented for the ILD baseline design with the inner ECAL radius  $R_{\text{ECAL}}^{\text{inner}} = 1843$  mm and for two models of smaller ILD with  $R_{\text{ECAL}}^{\text{inner}} = 1615$  and 1450 mm. The probability does not include the efficiency of charged  $\pi^+$  reconstruction, which is taken to be 100%. The off-diagonal values correspond to the probabilities of wrong reconstruction. For some events the decay mode could not be determined (either  $M_{\text{reco}}$  is larger than the tau-lepton mass or the event is not accepted by any classifier, as explained in Sec. 2.3), therefore the sum of the probabilities in columns and rows do not reach 100%. The reconstruction of two tau-leptons in  $Z^0 \rightarrow \tau^+ \tau^- (\gamma)$  events is performed indepen-

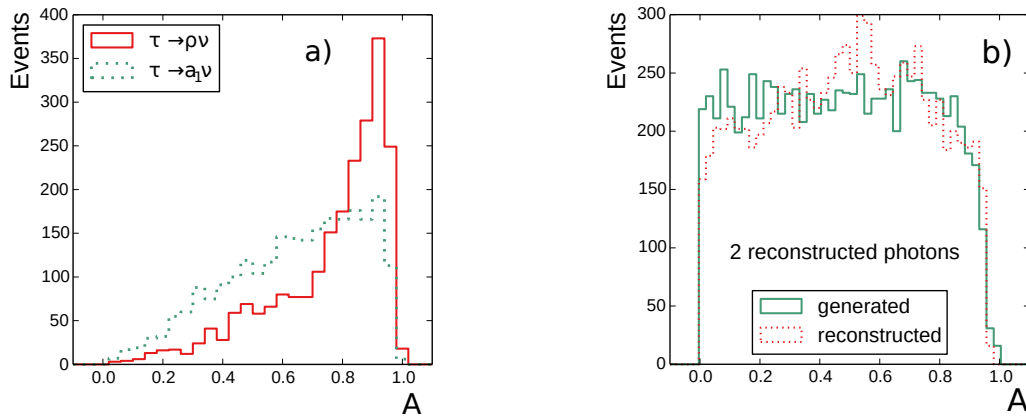


Fig. 1: The photon energy asymmetry  $A = (E_{\gamma}^{\max} - E_{\gamma}^{\min}) / (E_{\gamma}^{\max} + E_{\gamma}^{\min})$  in the case of three (a) and two (b) reconstructed photons. Solid and dashed curves are for (a): two decay modes  $\tau^+ \rightarrow \rho^+ \bar{\nu}_{\tau}$  and  $\tau^+ \rightarrow a_1^+ \bar{\nu}_{\tau}$ , (b): for the generated (Monte Carlo true) and measured energies, respectively.

dently, so that a failure to reconstruct one does not affect the other. The errors are purely statistical.

The correct reconstruction probability is close to 90% for  $\rho^+ \bar{\nu}_{\tau}$  and  $a_1^+ \bar{\nu}_{\tau}$  and above 95% for  $\pi^+ \bar{\nu}_{\tau}$  decays. For the smallest ILD with  $R_{\text{ECAL}}^{\text{inner}} = 1450$  mm the degradation of the probabilities compared to the baseline design is less than 2%.

For smaller ILD model there is an option to compensate the slightly degraded jet and track momentum resolution by a higher magnetic field. This increases the bending of the charged tracks and hadron-hadron and hadron-photon separation in the jets. Therefore, we also simulated the ILD performance with the magnetic field increased from the nominal 3.5 to 4 T. The corresponding reconstruction probabilities are shown in Fig. 3. The improvement is marginal and is less than 1%. This demonstrates that the failure rate is dominated by the photon reconstruction which is almost independent of the magnetic field.

The photon clusters from the decays of energetic  $\pi^0$ 's often overlap and this degrades the  $\pi^0$  mass resolution. The effect is stronger for smaller ILD ECAL with less photon separation. We study this effect using a sample with two reconstructed photons dominated by  $\rho^+ \bar{\nu}_{\tau}$  ( $\rho^+ \rightarrow \pi^+ \pi^0$ ) decays and therefore having more energetic  $\pi^0$ . Fig. 4a shows that the reconstructed invariant mass of  $\pi^0$  increases with its energy. This is explained by the fact that the GARLIC algorithm splits the overlapping showers geometrically into two disjoint groups of neighboring hits, neglecting the fact that some part of the cluster energy can propagate into the area of another cluster. This overestimates the distance between the cluster barycenters and the opening angle between the photons. The distribution in Fig. 4a

is fit to a parabolic function and the corresponding correction is applied to recover the nominal  $\pi^0$  mass at all energies. The resulting mass resolution, shown in Fig. 4b, has a symmetric shape. The relative  $\pi^0$  mass resolution is below 10% for all considered ILD models. The difference between the nominal and the smallest ILD models is about 1%.

A proper reconstruction of the tau decay modes together with a good momentum measurement of the decay products is mandatory to reconstruct the tau spin states in the measurement of the Higgs boson CP state in the decay  $H^0 \rightarrow \tau^+ \tau^-$ . The high probability of the correct decay mode reconstruction demonstrated in this paper shows the full potential of ILD even with the reduced size for such a measurement.

**Acknowledgements** The authors would like to thank Dr. Daniel Jeans, University of Tokyo for the help with the GARLIC package used in this study. This work is funded by the Physics Department of École polytechnique, Palaiseau, France and the “Physique des deux Infinis et des Origines” (P2IO) program.

## References

1. A. Heister *et al.* (ALEPH collaboration), Eur. Phys. J. C **20**, 401 (2001), arXiv:0104038 [hep-ex].
2. See, for example, the paper S. Berge, W. Bernreuther, H. Spiesberger, Phys.Lett. B **727** 488, (2013), arXiv:1308.2674 [hep-ph] and many references therein.
3. J.-C. Brient and H. Videau, proceedings of “APS/DPF/DBP Summer Study on the Future of Particle Physics” (Snowmass, Colorado, 2002), arXiv:hep-ex/0202004.
4. M. A. Thomson, Nucl. Instrum. Meth. A **611**, 25 (2009), arXiv:0907.3577 [physics.ins-det].

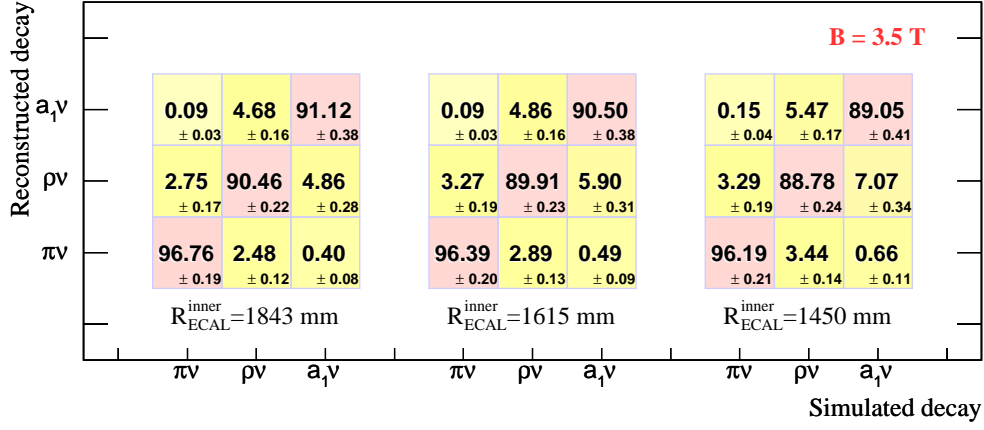


Fig. 2: The probability of the correct and wrong reconstruction of the tau decay modes  $\tau^+ \rightarrow \pi^+ \bar{\nu}_\tau$ ,  $\rho^+ \bar{\nu}_\tau$  and  $a_1^+ \bar{\nu}_\tau$  in percent, obtained for Si-W ECAL inner radius (from left to right)  $R_{\text{ECAL}}^{\text{inner}} = 1843$  (baseline), 1615 and 1450 mm and with the nominal magnetic field of 3.5 T. Only the statistical uncertainties are shown.

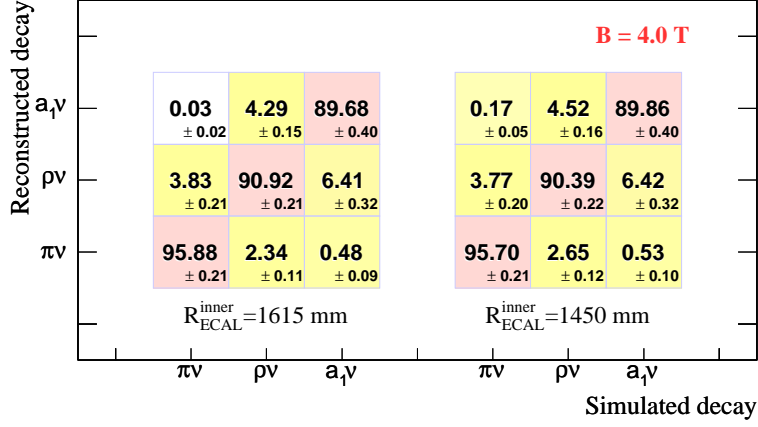


Fig. 3: The same as in Fig. 2, but for the magnetic field of 4 T.

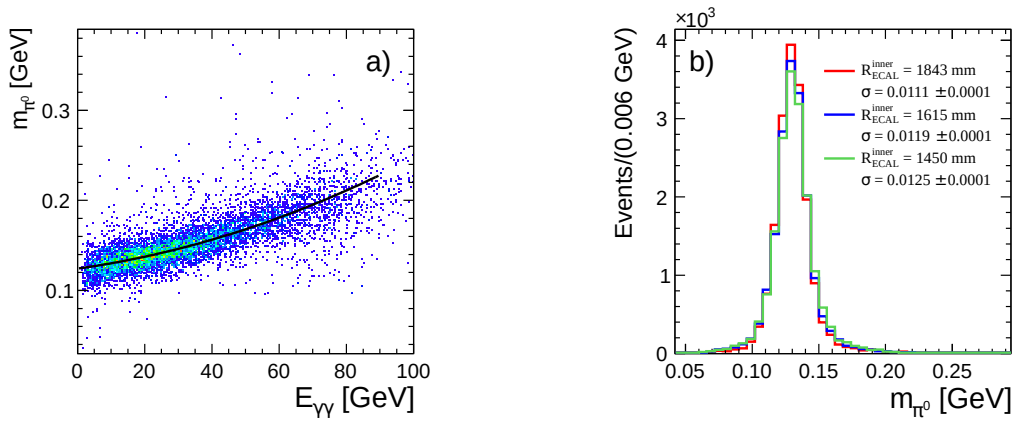


Fig. 4: Left: the dependence of the reconstructed mass of  $\pi^0$  on its energy before the correction. The black curve shows the parabolic fit. Right: the corrected  $\pi^0$  mass and the resolution for ILD with three different ECAL radii.

- 
5. The ILD Concept Group, “ILD Letter of Intent”, DESY 2009-87, KEK 2009-6 (2010), arXiv:1006.3396 [hep-ex].
  6. T. Behnke *et al.*, “The ILC Technical Design Report”, vol. 4 (International Linear Collider, 2013), arXiv:1306.6329 [physics.ins-det].
  7. P. M. de Freitas and H. Videau, “Detector simulation with MOKKA / GEANT4: Present and future”, proceedings of “International Workshop on Linear Colliders” (LCWS 2002, Jeju Island, Korea), 26-30.
  8. S. Agostinelli *et al.*, Nucl. Instrum. Meth. A **506**, 250 (2003), SLAC-PUB-9350, FERMILAB-PUB-03-339.
  9. T. H. Tran, proceedings of “International Workshop on Future Linear Colliders” (LCWS13, Tokyo, Japan), arXiv:1404.3173 [physics.ins-det].
  10. S. Jadach, J.H. Kühn, Z. Was, Comput. Phys. Commun. **64**, 275 (1990).
  11. K.A. Olive *et al.*, Chin. Phys. C **38**, 090001 (2014).
  12. M. Reinhard, J.-C. Brient, proceedings of “International Linear Collider Workshop” (LCWS08 and ILC08, Chicago, Illinois), arXiv:0902.3042 [hep-ex].
  13. D. Jeans, J.-C. Brient and M. Reinhard, J. Instrum. **7**, P06003 (2012), arXiv:1203.0774 [physics.ins-det].
  14. M. Ruan, D. Jeans, V. Boudry, J-C. Brient and H. Videau, Phys. Rev. Lett. **112**, 012001 (2014), arXiv:1312.7662 [physics.ins-det].